Springer

Journal of Mechanical Science and Technology 22 (2008) 2122~2133

Journal of Mechanical Science and Technology

www.springerlink.com/content/1738-494x
DOI 10.1007/s12206-007-1218-z

# Application of non-stationary signal characteristics using wavelet packet transformation †

Sang-Gil Park, Hyoun-Jin Sim, Hae-Jin Lee and Jae-Eung Oh*

*School of Mechanical Engineering, Hanyang University, 17 Haengdang-Dong, Seongdong-Gu, Seou1, 133-791, Korea*

(Manuscript Received October 4, 2007; Revised November 9, 2007; Accepted December 11, 2007)

**Abstract**

Although Fourier-based methods have been standard methods for frequency analysis, they are not well suited for the analysis of nonlinear or non-stationary systems due to their time-varying natures. Thus, in this paper, a wavelet packet-based technique, which calculates time-varying coherence functions for input/output relationships, is developed. The developed method uses the Coiflet wavelet that has been widely used in signal processing. It is applied to obtain the time-varying coherence function, and to detect the impulse signal from the impulse-embedded signal such as an automobile sound/vibration signal with an external impact caused by a collision or passing over rough terrain. Some characteristics of non-stationary behavior such as the wavelet packet coefficients, maximum phase plane (MPP) analysis and fault detection are also demonstrated. The method gives promising results of non-stationary input-output systems, and so may be used as an effective tool for condition monitoring or fault detection area.

*Keywords*: Wavelet packet; Signal processing; Non-stationary signal; MISO(Multiple Input/Single Output)

## 1. Introduction

For linear systems, Fourier-based analysis gives a good estimate of input-output relationships[1-4]. However, these methods are not well applicable to non-stationary systems, since the frequency content of a response varies with time, and 'averaging' over a large number of data windows smears the response characteristics. Thus, it is well known that Fourier based sound/vibration signal analysis exhibits several weaknesses[5, 6]. For the Fourier based input characterization to be practical, the input signals must contain a frequency spectrum rich enough to contain the structural frequency components of interest. And the FFT offers the frequency components of the entire signal, but not their occurrences in specific time intervals, hence making different signals indistinguishable as long as their spectral density is the same[7].

From a mathematical point of view, this FFT property may be linked to the fact that the windowed FFT cannot be represented in terms of orthogonal basis functions[8, 9].

To overcome this, the Short Time Fourier Transform (STFT) and Wigner-Ville distribution have been popular methods for non-stationary signal analysis. And the wavelet analysis is increasingly applied in these days.

It also demonstrates the possibility of early detection of a defective system by using both the wavelet packet method and the coherence analysis of a MISO(Multiple Input/Single Output) system.

The objective of this paper is to demonstrate the wavelet packet-based coherence function and to detect an impulse or a transient signal that is embedded in a non-stationary signal.

A number of applications of wavelets for transient or non-stationary signals from mechanical systems have been introduced in the area of fault detection and

† This paper was recommended for publication in revised form by Associate Editor Yeon June Kang

*Corresponding author. Tel.: +82 2 2220 0452 , Fax.: +82 2 2299 3153
E-mail address: jeoh@hanyang.ac.kr

diagnosis[10, 11], and a few other authors have explored the properties of wavelet-based frequency response function for an input-output system. Staszewski and Giacomin have analyzed acceleration transmissibilities across an automobile seat for transient and non-stationary data. Similar techniques have been applied to the cross wavelet analysis for a Duffing oscillator by Kyprianou and Staszewski[12].

Wavelets, which are mainly used as mathematical tools for analyzing time series or images, are a relatively new method of analyzing time series where the formal subject dates back to the 1980s. But in many aspects wavelets are the synthesis of older ideas with new elegant mathematical results and efficient computational algorithms. Wavelet analysis is, in some cases, complementary to existing analysis techniques (e.g., correlation and spectral analysis), and, in other cases, is capable of solving problems where little progress can be made without using the wavelets.

A wavelet packet is a generalization of a wavelet such that each octave frequency band of the wavelet spectrum is further subdivided into finer frequency bands by using the two-scale relations repeatedly.

Wavelet packets were introduced by Coifman et al.[13] by generalizing the link between multiresolution approximations and wavelets.

The properties of a non-stationary random process are generally time-varying functions that can be determined only by performing instantaneous averages over the ensemble of sampled functions forming the process. In practice, it is often not feasible to obtain a sufficient number of sample records to permit the accurate measurement of properties by ensemble averaging. This fact has made it difficult to develop practical techniques for measuring and analyzing non-stationary random data, especially in the area of system identification.

In many cases, a set of time series is non-stationary and correlated with each other so that the Fourier method may not be successfully applied. Thus, in this paper, we introduce a wavelet packet method based on the coherence analysis of a MISO system, and demonstrate the possibility of fault diagnosis of a system that produces an impulse or transient characteristics.

## 2. Theory

### *2.1 Wavelet packet transform*

Discrete wavelet packet transform (DWPT) is derived from a simple modification of the pyramid algorithm for the discrete wavelet transform (DWT). The $J-1$ th level decomposition splits $[0, 1/2]$ into $N/2 = 2^{J-1}$ equal intervals, where $[\ ]$ denotes the closed interval. When $j = 1, \ldots, J-1$, the resulting DWPT yields a 'time-frequency' decomposition because each DWPT coefficient can be localized to a particular band of frequencies and a particular interval of time.

Let $\mathbf{W}(t) = \mathbf{w}\mathbf{X}(t)$ represent the wavelet coefficients obtained by transforming $\mathbf{X}(t)$ ( $t = 0, 1, \ldots, N-1$, we simply denote it $\mathbf{X}$ ) using the $N \times N$ orthonormal DWT matrix $\mathbf{w}$. For convenience, we assume that $N = 2^J$ for some integer $J$.

If scaling filter $g_l$ is given, the required second filter (wavelet filter) is the 'quadrature mirror filter' (QMF) $h_l$ that corresponds to $g_l$:

$$h_l = (-1)^l g_{L-1-l} \tag{1}$$

at level $j$:

$$h_{j,l} = \sum_{k=0}^{L_{j-1}-1} g_{l-2k} h_{j-1,k} \qquad g_{j,l} = \sum_{k=0}^{L_{j-1}-1} g_{l-2k} g_{j-1,k} \tag{2}$$

And the wavelet filter must satisfy the following three basic properties:

$$\sum_{l=0}^{L-1} h_l = 0\,, \quad \sum_{l=0}^{L-1} h_l^2 = 1\,, \quad \sum_{l=0}^{L-1} h_l h_{l+2n} = \sum_{l=-\infty}^{\infty} h_l h_{l+2n} = 0 \tag{3}$$

Fig. 1 illustrates this transformation from a filtering point of view.

For the general $j$ th stage of the pyramid algorithm, where $j = 1, \ldots, J$. With $\mathbf{V}_{0,t}$ defined to be $\mathbf{X}_t$, the $j$ th stage input is $\mathbf{V}_{j-1,t}$ ($t = 0, \ldots, N_{j-1} - 1$, where $N_j \equiv N/2^j$). The elements of this input are the scaling coefficients associated with averages over scale $\lambda_{j-1} = 2^{j-1}$. And the $j$ th stage

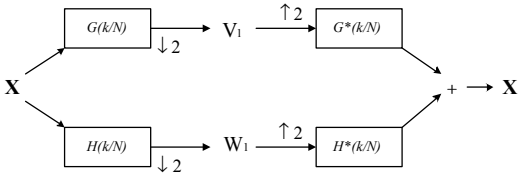


Fig. 1. Flow diagram illustrating analysis and synthesis of $\mathbf{X}$. ('↓2' indicates downsampling by two and '↑2' indicates upsampling by two.)

outputs are the $j$ th level wavelet and scaling coefficients:

$$\mathbf{W}_{j,t} = \sum_{l=0}^{L-1} h_{j,l}\mathbf{X}_{2^j(t+1)-1-l} \qquad \mathbf{V}_{j,t} = \sum_{l=0}^{L-1} g_{j,l}\mathbf{X}_{2^j(t+1)-1-l} \tag{4}$$

Disjoint dyadic decomposition is defined as the process that performs the splitting by using both $G(\cdot)$ and $H(\cdot)$ in the table structure as described in Fig. 2.

Ordering the filtering operations seems to be more intuitive because the upper branch of each split in the flow diagram, Fig. 1, always goes into $G(\cdot)$, while the lower branch into $H(\cdot)$. Wickerhauser[6] refers to this as 'natural ordering'. However, frequency ordering is no longer directly reflected in the second index.

The above results can be easily generalized, and the following two rules are must be satisfied.

[1] If $n$ in $\mathbf{W}_{j-1,n}$ is even, the low-pass filter $G(\cdot)$ is used to obtain $\mathbf{W}_{j,2n}$ and the high-pass filter $H(\cdot)$ to obtain $\mathbf{W}_{j,2n+1}$.

$$\mathrm{W}_{j,2n} = \mathrm{A}_j \mathrm{W}_{j-1,n} \text{ and } \mathrm{W}_{j,2n+1} = \mathrm{B}_j \mathrm{W}_{j-1,n} \tag{5}$$

[2] If $n$ is odd, $H(\cdot)$ is used to obtain $\mathbf{W}_{j,2n}$ and $G(\cdot)$ to obtain $\mathbf{W}_{j,2n+1}$.

$$\mathrm{W}_{j,2n} = \mathrm{B}_j \mathrm{W}_{j-1,n} \text{ and } \mathrm{W}_{j,2n+1} = \mathrm{A}_j \mathrm{W}_{j-1,n} \tag{6}$$

With these rules, $2^j$ vectors can be constructed

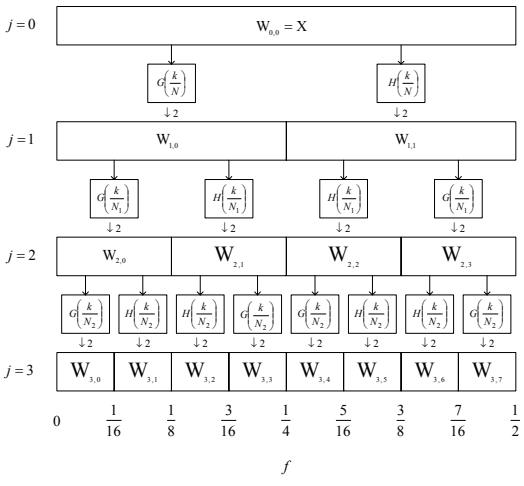


Fig. 2. Flow diagram illustrating the analysis of $\mathbf{X}$ into $\mathbf{W}_{2,0}$, $\mathbf{W}_{2,1}$, $\mathbf{W}_{2,2}$ and $\mathbf{W}_{2,3}$. In the above recall that $N_1 = N/2$.

at level $j$, namely, $\mathbf{W}_{j,n}$, $n = 0, \ldots, 2^j - 1$. The vector $\mathbf{W}_{j,n}$ is corresponding to the frequencies in the interval $\left[n/2^{j+1}, (n+1)/2^{j+1}\right]$. This is demonstrated in Fig. 2, which shows the analysis process up to level 3. This figure is an example of a wavelet packet table. Since the starting point is the time series $\mathbf{X}$, it is convenient to define $\mathbf{W}_{0,0} \equiv \mathbf{X}$ so that $\mathbf{X}$ is associated with a $(j,n)$ doublet.

The transform that takes $\mathbf{X}$ to $\mathbf{W}_{j,n}$, for any $j$ between 0 and $J$ is called a discrete wavelet packet transform (DWPT). And it is an orthonormal transformation.

To compute the DWPT coefficients of level $j = 1,\ldots,J$, it recursively filters the DWPT coefficients at each previous stage. Let $\mathbf{W}_{j-1,n,t}$ represent the $t$ -th element of $\mathbf{W}_{j-1,n}$, $n = 0, \ldots, 2^j - 1$. Given this vector of which length is $N_j - 1$, the above two rules are used to produce the elements of $\mathbf{W}_{j,n}$, so that:

$$\mathbf{W}_{j,n,t} = \sum_{l=0}^{L-1} u_{n,l}\mathbf{W}_{j-1,\lfloor n/2 \rfloor, 2t+1-l \bmod N_{j-1}}, \quad t = 0,\ldots,N_j - 1 \tag{7}$$

where $u_{n,l} = \begin{cases} g_l, & \text{if } n \bmod 4 = 0 \text{ or } 3 \\ h_l, & \text{if } n \bmod 4 = 1 \text{ or } 2 \end{cases}$

and $\lfloor \cdot \rfloor$ denotes the 'integer part' operator.

Suppose that $u_{1,0,l} \equiv g_l$ and $u_{1,1,l} \equiv h_l$. For nodes $(j,n)$ with $j > 1$,

$$u_{j,n,l} \equiv \sum_{k=0}^{L-1} u_{n,k} u_{j-1,\lfloor n/2 \rfloor, l-2^{j-1}k} \tag{8}$$

Then for $j = 1,\ldots,J$, the elements of $\mathbf{W}_{j,n}$ can be written in terms of a filtering of $\mathbf{X}$ with appropriate downsampling,

$$\mathbf{W}_{j,n,t} = \sum_{l=0}^{L_j-1} u_{j,n,l}\mathbf{X}_{2^j\lfloor t+1 \rfloor - 1 - l \bmod N}, \quad t = 0,\ldots,N_j - 1 \tag{9}$$

For $j = 0$, the time width is unity, and the bandwidth is 1/2, which makes sense considering that DWPT is the identity transform for the level $j = 0$. In the case of the other extreme, i.e., the level $j = J$, DWPT of a series with length $N = 2^J$, the time width is $N$, and the bandwidth is $1/(2N)$.

### *2.2 Choice of wavelet*

In this paper, following filters are considered: Daubechies(D20) filter, Least asymmetric(L20) filter and Coiflet(C18,C24) filter (the number inside () denotes no. of taps).

Fig. 3 shows the scaling filter and wavelet filter of each of the four filters.

For the criteria of wavelet selection, the wavelet packet coefficients and statistical correlation coefficients are used; also, the eigenvalue cumulative index (ECI) is introduced as discussed below.

The new parameter ECI is obtained from the following procedure: (1) calculate the covariance matrix from wavelet packet coefficients; (2) solve the eigenvalue problem and make the eigenvalues in descending order; (3) cumulate the eigenvalues and divide by the total sum:

$$ECI_n = \frac{\sum_{u=0}^{n} |\lambda_u|}{\sum_{u=0}^{N-1} |\lambda_u|} \tag{10}$$

where, $|\lambda_0| \geq |\lambda_1| \geq \cdots \geq |\lambda_{N-2}| \geq |\lambda_{N-1}|$, $n = 0,1,\ldots,N-1$

The correlation coefficients[14] between inputs and output are defined as below. These values are listed in Table 1, for each filter.

$$\textit{Correlation coefficient},\ \rho = \frac{\sigma_{XY}^2}{\sigma_X \sigma_Y} \tag{11}$$

where,

$$\textit{Variance},\ \sigma_X^2 = E\left[(X - E(X)^2\right] = E(X^2) - (E(X))^2$$

$$\textit{Covariance},\ \sigma_{XY}^2 = E\left[(X - E(X))(Y - E(Y))\right]$$

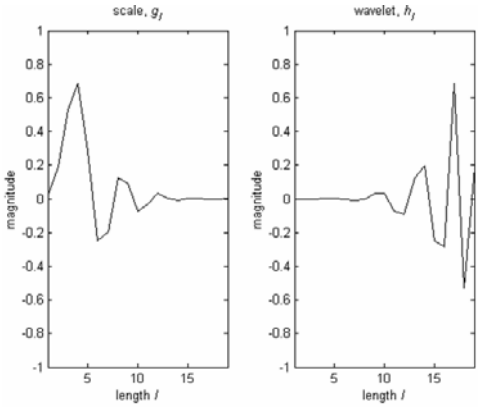


(a) D(20)

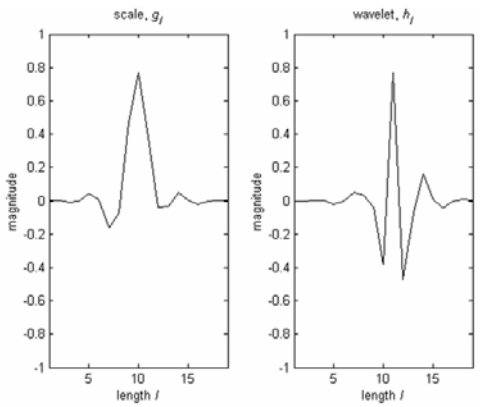


(b) LA(20)

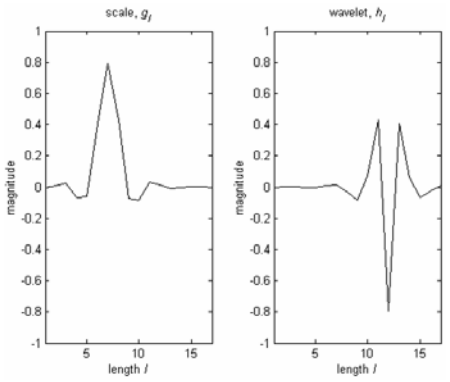


(c) C(18)

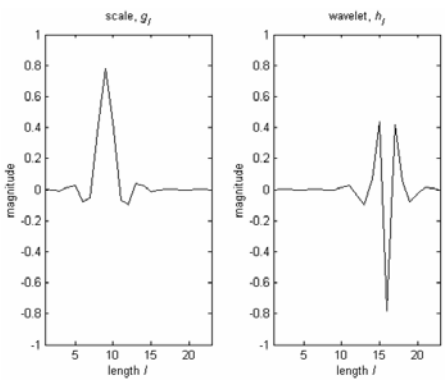


(d) C(24)

Fig. 3. Shape of selected filters.

As shown in Table 1, each filter has a different value of the correlation coefficients. C18 has the largest correlation coefficient and its value is 0.9561 for $x_2$. And it shows in the order of '$x_2 > x_1 > x_3$' on the whole.

The reference signal, for comparison, is shown in Fig. 7(a) (below). The mean value is –21.6 and the standard deviation is 1851.3. The wavelet packet coefficients of the reference signal are shown in Fig. 4 for each filter, and the eigenvalue cumulative indexes (ECI) are also shown in Fig. 5, respectively.

Table 1. Correlation coefficients between inputs and output for each filters.

| | $x_1$ | $x_2$ | $x_3$ |
|---|---|---|---|
| D20 | 0.5920 | 0.5132 | 0.1531 |
| LA20 | 0.5163 | 0.4738 | 0.0018 |
| **C18** | **0.8258** | **0.9561** | **0.2112** |
| C24 | 0.6726 | 0.8361 | 0.3962 |

In Figs. 4 and 5, the filter properties are very similar, so that the selection becomes difficult.

It can be seen that the correlation coefficients of the Coiflet (tap18) filter are the largest (refer to Table 1); thus the Coiflet filter C(18) is chosen.

The term 'Coiflets' was coined by Daubechies to acknowledge the role of R. Coifman in suggesting the idea to construct these filters. Coiflets provide an interesting fact to the Daubechies scaling and wavelet filters. They are obtained by specifying certain 'vanishing moment' conditions on a wavelet function that is entirely determined by the associated scaling filter. The idea is also to specify vanishing moment conditions on the associated scaling function. This construction produces an appealing set of wavelet filters with remarkably good phase properties.

The main feature is that the scaling function has vanishing moment properties. For example, $m$-th order Coiflets are:

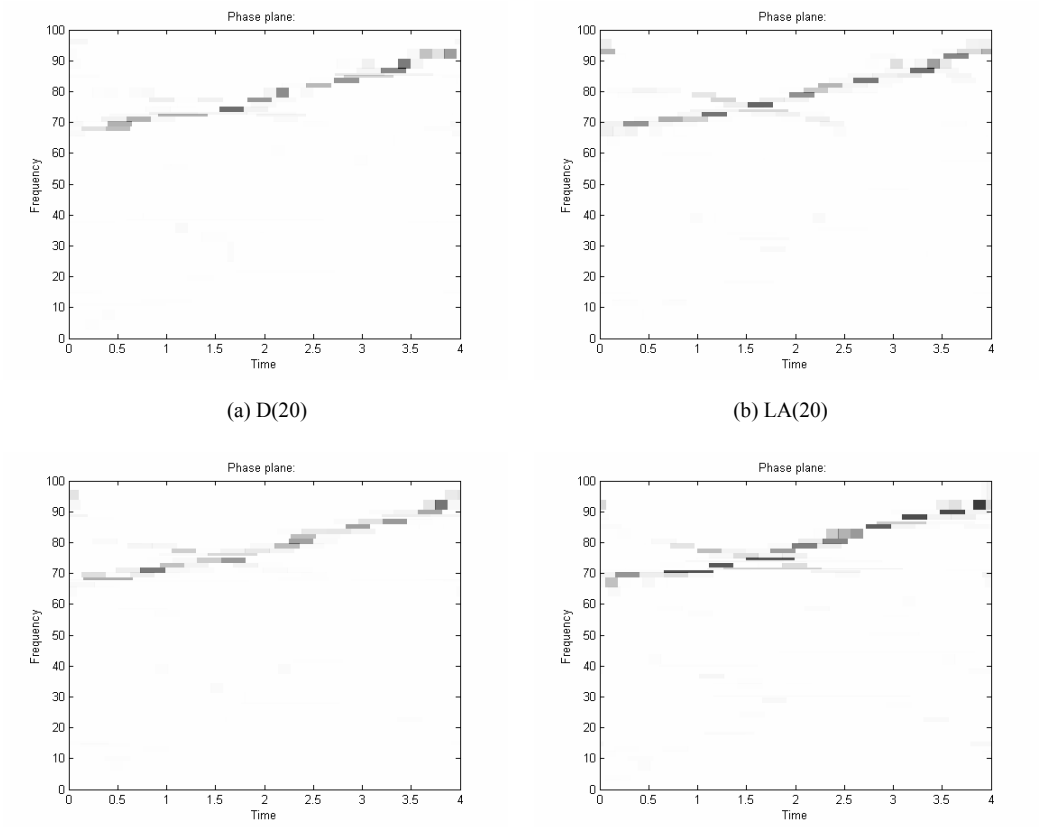


(a) D(20) (b) LA(20)

(c) C(18) (d) C(24)

Fig. 4. Wavelet packet analysis for reference signal of each filter.

Table 2. Sensor specifications.

| | $x_1$ | $x_2$ | $x_3$ | $y$ |
|---|---|---|---|---|
| Sensor type | accelerometer | microphone | microphone | Microphone |
| Position | On engine head | Air intake hose, engine side | Before resonator | Air intake hose, end side |
| Max. voltage | 1.4 V | 8 V | 1.03 V | 7.8 V |
| Calculation factor | - | 94dB / 0.063 V | 94dB / 0.001055 V | 94dB / 0.000965 V |
| DBR after calibration | - | 113.6 dB (118.1 rms) | 134.7 dB (140.7 rms) | 159.5 dB (164 rms) |

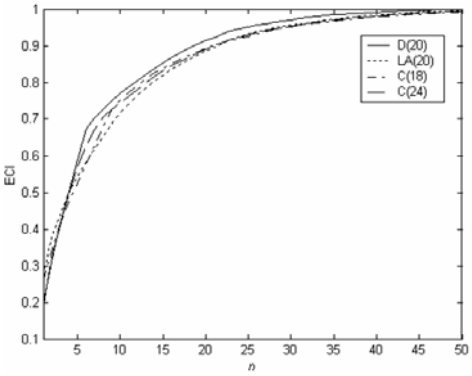


Fig. 5. Comparison of ECI with selected filters.

Fig. 6. Sensor position layout.

$$\int_{-\infty}^{\infty} t^p h(t)dt = 0, \quad p = 0,\ldots,m-1$$

$$\int_{-\infty}^{\infty} t^p g(t)dt = 0, \quad p = 1,\ldots,m-1$$

$$\int_{-\infty}^{\infty} h(t)dt = 1$$

So the wavelet and the scaling functions have an equal number of vanishing moments in this case. Note that such vanishing moments on the scaling filter also increase its symmetry.

## 3. Results

### *3.1 Coherence analysis*

Discrete time data are collected from a 1500cc passenger car that is accelerated from 70 Hz to 95 Hz (about 2,100 rpm ~2,850 rpm) in 4 seconds.

The sensor specifications and measurement points are illustrated in Table 2 and Fig. 6, respectively.

The measured time data are acceleration on the engine head( $x_1$ ), pressure on the engine side of the air intake hose( $x_2$ ), pressure on the point before the resonator( $x_3$ ) and pressure on the end side of the air intake hose( $y$ ). They are 1024 samples each and are shown in Fig. 7.

The results of wavelet packet analysis are shown in Fig. 8. It can be seen that $x_1$, $x_2$ and $y$ are the time varying signals, and $x_3$ is different from the other signals. A maximum phase plane (MPP) is introduced as the maximum values of the wavelet packet coefficients for each time. In these figures, the solid line is the MPP line. Fig. 9 shows the magnitude of MPP.

The non-stationarity of the output signal is checked, and the results of the wavelet packet transforms are shown in Fig. 10. Fig. 10 (a) is the wavelet packet output at 1.0 second, and Fig. 10 (b) is at 3.0 seconds. These figures show the frequency characteristics according to the time changes; the frequency components increase as the time elapse from 1 sec to 3 sec, which shows the rapid acceleration of the engine speed.

From these figures, it is shown that the output magnitude increases as the frequency increases.

For the coherence analysis, the mean of ordinary coherence function (OCF) is calculated. The overall OCFs are plotted in Fig. 11. The OCF values are 0.8973 for $x_1$, 0.8848 for $x_2$ and 0.2300 for $x_3$ with respect to the output $y$. $x_1$ and $x_2$ are greatly

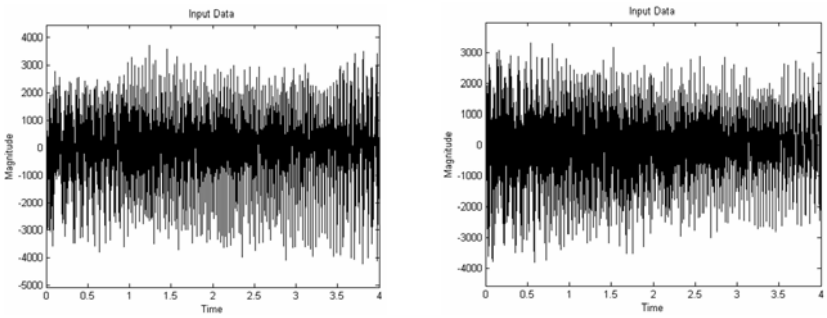


(a) $x_1$ (b) $x_2$

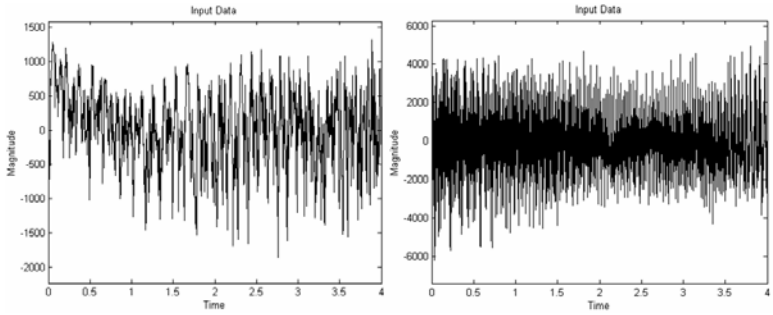


(c) $x_3$ (d) $y$

Fig. 7. Input and output time signals.

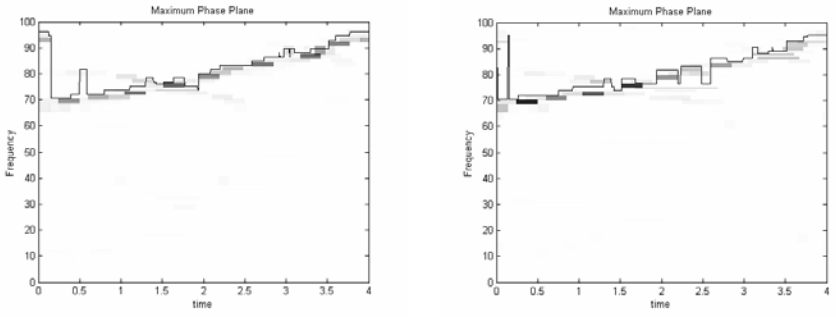


(a) $x_1$ (b) $x_2$

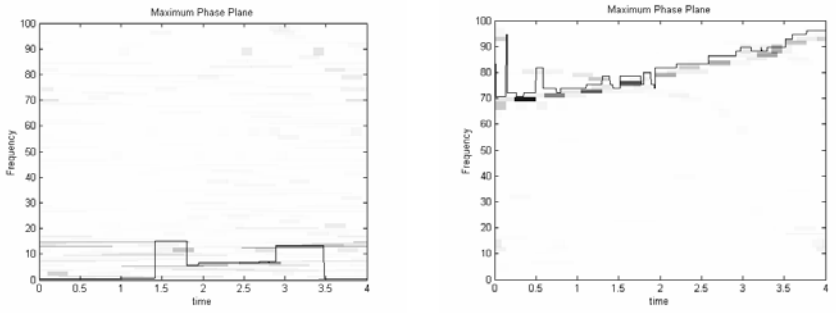


(c) $x_3$ (d) $y$

Fig. 8. Wavelet packet analysis of time signals.

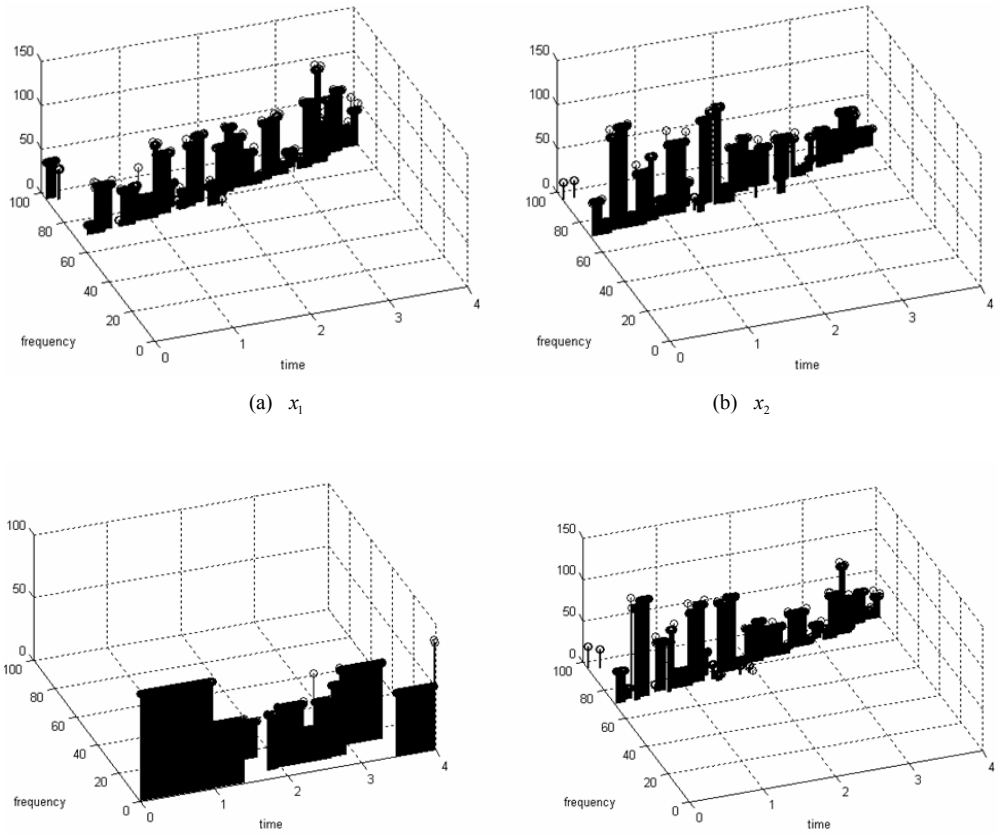


(a) $x_1$ (b) $x_2$

(c) $x_3$ (d) $y$

Fig. 9. Magnitude of MPP for each time-frequency plane.

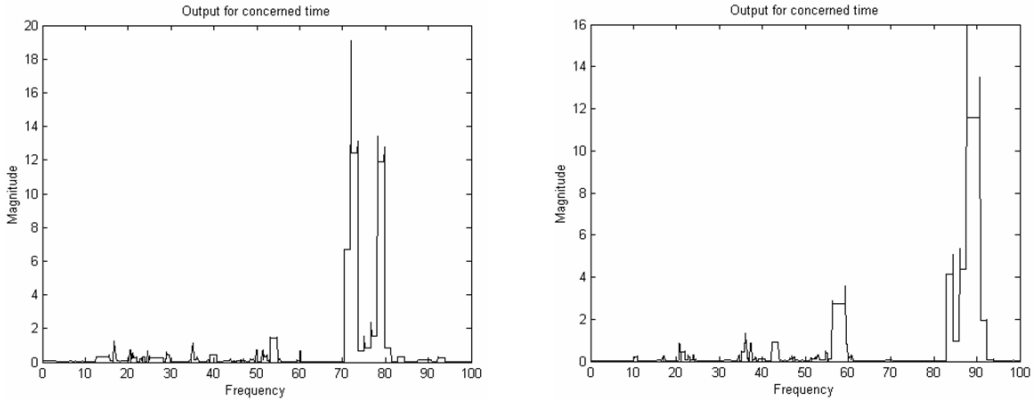


(a) at 1 sec (b) at 3 sec

Fig. 10. Wavelet packet transform of output signal at two different incidences.

correlated with the output, but $x_3$ is poorly correlated with the output. The overall coherences for the entire time span are shown in Fig. 12 and listed in Table 3 at each 0.5 second time step. It is shown that these are in good agreement with the results of the correlation coefficients shown in Table 1.

Table 3. Values of ordinary coherence function.

| | Mean of $\gamma_{1y}$ | Mean of $\gamma_{2y}$ | Mean of $\gamma_{3y}$ |
|---|---|---|---|
| **Overall** | **0.8973** | **0.8848** | **0.2300** |
| 0.0 sec | 0.6359 | 0.7213 | 0.4220 |
| 0.5 sec | 0.7848 | 0.8410 | 0.2024 |
| 1.0 sec | 0.8973 | 0.8848 | 0.2300 |
| 1.5 sec | 0.7598 | 0.7966 | 0.3014 |
| 2.0 sec | 0.9709 | 0.9800 | 0.3560 |
| 2.5 sec | 0.7869 | 0.9060 | 0.2217 |
| 3.0 sec | 0.9007 | 0.8281 | 0.1797 |
| 3.5 sec | 0.7223 | 0.7350 | 0.3820 |
| 4.0 sec | 0.6452 | 0.7240 | 0.4187 |

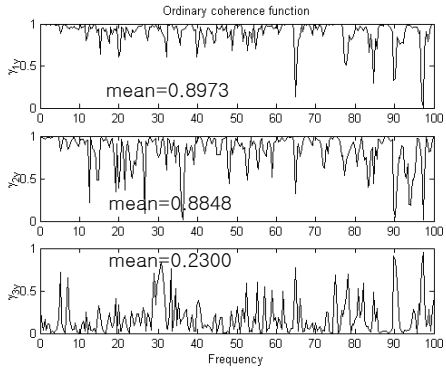


Fig. 11. Ordinary coherence function.

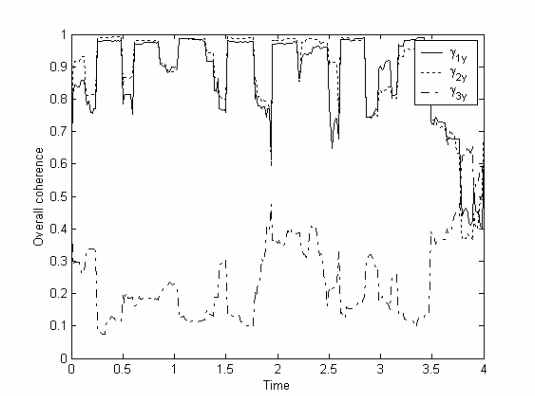


Fig. 12. Overall coherence function for time sweep.

### *3.2 Degree of non-stationarity.*

The non-stationarity is examined by the slope of maximum phase plane. Linear regression is used since the MPP are linearly increased. Fig. 13 shows the combination of MPP and regression line of the output signal.

Regression for each input and output signal is obtained:

$$\text{input} \quad x_1 : f = 5.09763\,t + 72.05005$$
$$x_2 : f = 6.09104\,t + 68.74956$$
$$x_3 : f = 1.67095\,t + 2.09893$$
$$\text{output} \quad y : f = 6.18407\,t + 69.41155$$

where, $t$ is time and $f$ is approximated frequency at $t$.

This shows that the slope of each signal is 5.09763 for $x_1$ and 6.09104 for $x_2$, respectively, and these values are similar to the output slope, 6.18407. But the slope of $x_3$ is 1.67095, which indicates distinctive frequency variations correspond with other signals. Thus, it can be concluded that the signals, except $x_3$, are about 5~6.2 frequency increment for 1 second, and so these signals can be considered as non-stationary signals.

### *3.3 Effect of impulse*

An impulse is added to the measured time varying signal (engine head) at 1 second.

Fig. 14 shows the effect of the impulse, where the impulse appears as low frequency component. The vertical line represents the magnitude of the impulse.

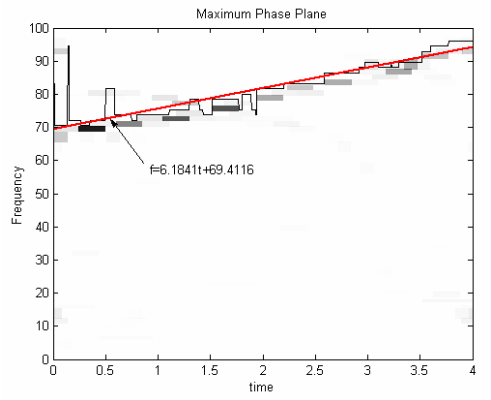


Fig. 13. MPP regression for checking the non-stationarity.

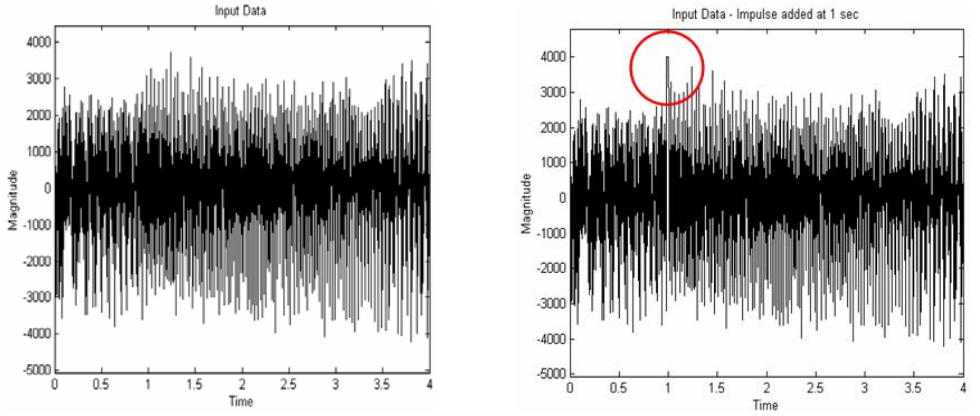


(a) Original data(left) and impulse added data(right)

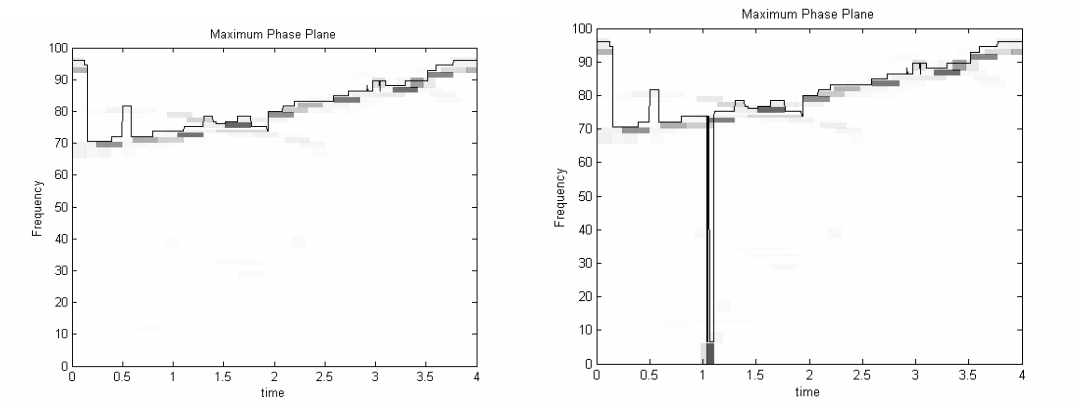


(b) Wavelet coefficients and maximum phase plane for (a)

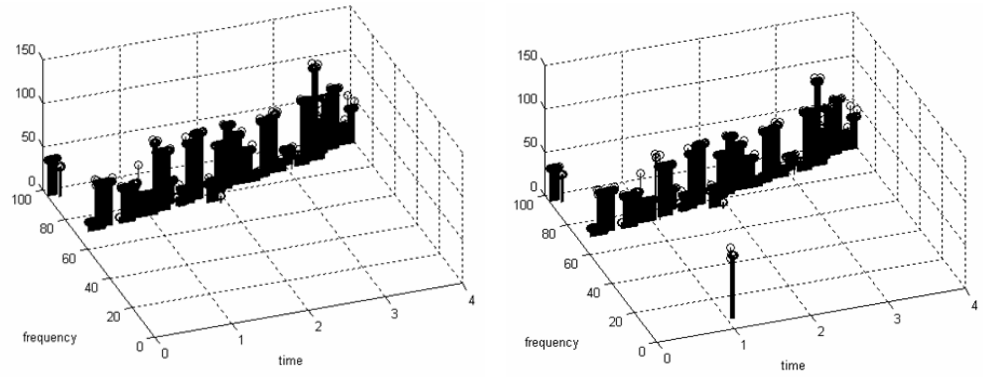


(c) Magnitude of maximum phase plane for (a)

Fig. 14. Comparison with original and impulse added signals.

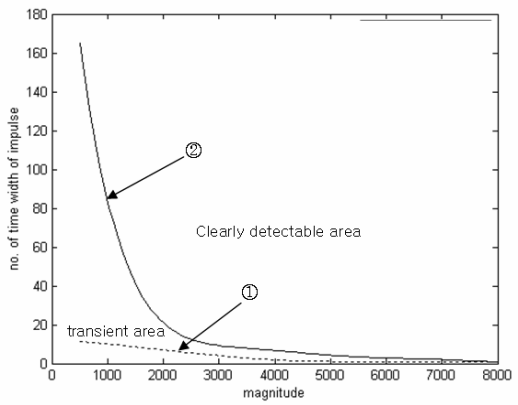


Fig. 15. Effect of magnitude and time width of impulse.

Thus, the diagnosis of the system is illustrated by means of a possible on-line condition monitoring of non-stationary signals.

Fig. 15 demonstrates the possibility of fault detection from the impulse added signal. The energy increment ratio (EIR) is defined below:

$$EIR = \frac{\sqrt{\int x'^2 dt} - \sqrt{\int x^2 dt}}{\sqrt{\int x^2 dt}} \times 100\ (\%) \qquad (12)$$

where, $x(t)$ = original signal, and $x'(t)$ =impulse added signal.

This describes the energy difference between 'impulse added signal energy squared' and 'original signal energy squared', and this is used as the fault detection parameter.

The minimum detectable area is about 0.5%, i.e., only appearing in wavelet packet analysis (in Fig. 15, line ①), and the clearly detectable area is about 1.5%, which appears in both the wavelet packet analysis and the magnitude of MPP (in Fig. 15, line ②).

## 4. Conclusion

For a given non-stationary data, we have compared eigenvalue cumulative index and correlation coefficients for the Daubechies filter, Least asymmetric filter and Coiflet filters, respectively. The result of the wavelet shows similar values of ECI; however, the Coiflet filter is found to be especially efficient for correlation coefficients, so the Coiflet filter is used for the wavelet packet analysis.

For coherence analysis, the mean value of the ordinary coherence function (OCF) is calculated. It is shown that $x_1$ and $x_2$ are largely correlated with the output, whereas $x_3$ is poorly correlated with the output. This agrees with the results of correlation coefficients.

The maximum value of MPP at each time incidence and the corresponding regression equations was obtained to investigate the degree of non-stationarity; it is shown that the input $x_1$ and $x_2$ have large coherence to the output, while the input $x_3$ has little coherence to the output.

If an impulse is added, it appears as low frequency component. And, the diagnosis of the system is illustrated by means of a possible on-line condition monitoring of non-stationary signals.

The possibility of fault detection is demonstrated by analyzing the impulse added signal. The energy increment ratio (EIR) is used. This describes the energy difference between 'impulse added signal energy squared' and 'original signal energy squared', and is used as the fault detection parameter.

If the energy increment ratio(EIR) is between 0.5%~1.5%, the effect of the impulse is noticeable. If it is greater than 1.5%, it can be detected regardless of the magnitude and time duration of the impulse.

The minimum detectable area is about 0.5%, only appearing in the wavelet packet analysis, and the clearly detectable area is about 1.5%, which appears in both the wavelet packet analysis and the magnitude of MPP.

Finally, a method of system identification has been developed by combining the wavelet packet analysis method and the coherence analysis method. It was successfully applied to a non-stationary signal by means of fault diagnosis.

## Acknowledgment

This work was supported by the Second Brain Korea 21 Project in 2008.

## References

[1] J. S. Bendat, System Identification From Multiple Input/Output Problems, *Journal of Sound and Vibration*, 49 (3) (1981) 293-308.

[2] J. S. Bendat, Modern Analysis Procedures for Multiple Input/Output Problems, *Journal of the Acoustical Society of America*, 68 (2) (1980) 498-503.

[3] J. S. Bendat and A. G. Piersol, Decomposition of Wave Forces into Linear and Nonlinear Compo-

nents, *Journal of Sound Vibration*, 106 (3) (1986) 391-408.

[4] J. S. Bendat and A. G. Piersol, *Engineering Applications of Correlation and Spectral Analysis,* 2nd Ed., John Wiley & Sons, Inc., (1993)..

[5] J. W. Cooley and J. W. Tukey, An Algorithm for the Machine Calculation of Complex Fourier Series, *Mathematics of Computation*, 19 (90) (1965) 297-301.

[6] A. N. Robertson, K. C. Park and K. F. Alvin, Extraction of Impulse Response Data via Wavelet Transform for Structural System Identification, *ASME Journal of Vibration and Acoustic*, 120 (1998) 252-260.

[7] A. N. Robertson, K. C. Park and K. F. Alvin, Identification of Structural Dynamic Models Using Wavelet-Generated Impulse Response Data, *ASME Journal of Vibration and Acoustic*, 120 (1998) 261-266.

[8] D. E. Newland, *An Introduction to Random Vibrations, Spectral & Wavelet Analysis*. 3rd Ed. Longman Pub, (1993).

[9] I. Daubechies, Orthonormal bases of compactly supported wavelets, *Comm. Pure and Appl. Math.*, 1 (41) (1988) 909-996.

[10] I. Daubechies, *Ten Lectures on Wavelets*, CBMS/NSF Series in Applied Mathematics #61, SIAM Publ, (1992).

[11] W. J. Wang and P. D. McFadden, Application of Wavelets to Gearboxes Vibration Signals for Fault Detection, *Journal of Sound and Vibration*, 192 (5) (1996) 927-939.

[12] J. Lin and L. Qu, Feature Extraction Bases on Morlet Wavelet and Its Application for Mechanical Fault Diagnosis, *Journal of Sound and Vibration*, 234 (1) (2000) 135-148.

[13] A. Kyprianou and W. J. Staszewski , On Cross Wavelet Analysis of the Duffing Oscillator, *Journal of Sound and Vibration*, 228 (1) (1999) 199-210.

[14] R. R. Coifman, M. Meyer and M. V. Wickerhauser, *Wavelet Analysis and Signal Processing. In Wavelets and their Applications*, Boston, Jones and Barlett, (1992).

[15] W. J. Staszewski and J. Giacomin, Application of the Wavelet Based FRFs to the analysis of NonStationary Vehicle Data, *Proceedings of 15th International Modal Analysis Conference*, 1 (4) (1997) 425-431.

[16] R. G. Brown and P. Y. C. Hwang, *Introduction to Random Signals and Applied Kalman Filtering*, 3rd Ed. John Wiley & Sons, (1997).

[17] J. W. Cooley and J. W. Tukey, An Algorithm for the Machine Calculation of Complex Fourier Series, *Mathematics of Computation*, 19 (90) (1965) 297-301.

[18] J. E. Oh, S. H. Suh and M. S. Kang, Application of Multi-Dimensional Spectral Analysis for Noise Source Identification on Gasoline Engine, *KSME*, 10 (4) (1986) 442-449.

[19] J. E. Oh, J. H. Cho, J. E. Song and H. S. Lee, The Identification of Generation Mechanism of Noise and Vibration and Transmission Characteristics for Engine System, *KSME*, 21 (7) (1997) 1127-1140.

[20] M. V. Wickerhauser, *Adapted Wavelet Analysis from Theory to Software*, Wellesley, Massachusetts, (1994).

**Jae-Eung Oh** received his B.S. degree of mechanical engineering at Hanyang University in 1975 and his M.S. degree of Safety Engineering at Yokohama National University in 1980.
He then went on to receive his doctorate degree in environmental engineering from Tokyo
Institute of Technology in 1983. He is currently the Vice President of KSNVE.